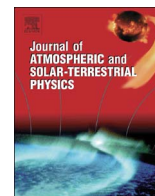




Contents lists available at ScienceDirect

Journal of Atmospheric and Solar–Terrestrial Physics

journal homepage: www.elsevier.com/locate/jastp

Impacts of a sudden stratospheric warming on the mesospheric metal layers

Wuhu Feng^{a,b}, Bernd Kaifler^c, Daniel R. Marsh^d, Josef Höffner^e, Ulf-Peter Hoppe^f, Bifford P. Williams^g, John M.C. Plane^{a,*}^a School of Chemistry, University of Leeds, Leeds, UK^b NCAS, School of Earth and Environment, University of Leeds, Leeds, UK^c Institute of Atmospheric Physics, German Aerospace Center (DLR), Oberpfaffenhofen, Germany^d National Center for Atmospheric Research, Boulder, Colorado, USA^e Leibniz-Institute of Atmospheric Physics, Kühlungsborn, Germany^f The Arctic University of Norway, Tromsø, Norway^g GATS, Inc., Boulder, Colorado, USA

ARTICLE INFO

Keywords:

Sudden stratospheric warming

Mesospheric metal layers

Lidar observations

Whole atmosphere model

ABSTRACT

We report measurements of atomic sodium, iron and temperature in the mesosphere and lower thermosphere (MLT) made by ground-based lidars at the ALOMAR observatory (69°N, 16°E) during a major sudden stratospheric warming (SSW) event that occurred in January 2009. The high resolution temporal observations allow the responses of the Na and Fe layers to the SSW at high northern latitudes to be investigated. A significant cooling with temperatures as low as 136 K around 90 km was observed on 22–23 January 2009, along with substantial depletions of the Na and Fe layers (an ~80% decrease in the column abundance with respect to the mean over the observation period). The Whole Atmosphere Community Climate Model (WACCM) incorporating the chemistry of Na, Fe, Mg and K, and nudged with reanalysis data below 60 km, captures well the timing of the SSW, although the extent of the cooling and consequently the depletion in the Na and Fe layers is slightly underestimated. The model also predicts that the perturbations to the metal layers would have been observable even at equatorial latitudes. The modelled Mg layer responds in a very similar way to Na and Fe, whereas the K layer is barely affected by the SSW because of the enhanced conversion of K⁺ ions to K atoms at the very low temperatures.

1. Introduction

Sudden Stratospheric Warmings (SSWs) are large-scale dynamical events which cause a rapid temperature increase (> 20 K) in the polar stratosphere and, in the case of major warmings, a reversal of the zonal-mean zonal wind at high latitudes and heights around 10 hPa (McInturff, 1978; Christiansen, 2001). SSWs typically last for a few days or weeks (Butler et al., 2015). They cause large variations in the gravity wave flux (Yamashita et al., 2010; Vincent, 2015), which can strongly affect vertical coupling over a large range of altitudes from the stratosphere down to the surface (Baldwin and Dunkerton, 2001) and up to thermosphere (Goncharenko and Zhang, 2008; Chau et al., 2009; Yamazaki et al., 2015). There is increasing evidence that SSWs have a significant impact on surface weather (Baldwin and Dunkerton, 2001) and potential effect on ocean circulation (O'Callaghan et al., 2014). SSWs can also induce changes in atmospheric composition and hence radiative transfer (Flury et al., 2009). Many studies have been conducted to investigate perturbations to ozone and other chemical

species in the middle atmosphere caused by SSWs (Rose and Brasseur, 1989). Damiani et al. (2014) reported a significant influence on composition in the polar upper stratosphere and lower thermosphere after a major SSW event. There can also be a substantial neutral density drop in the thermosphere during a SSW (Liu et al., 2011). Marsh et al. (2013a) reported a model prediction of a large decrease in Na column during a SSW; subsequently, Dunker et al. (2015) used lidar measurements to confirm a large variation in temperature and Na density in the MLT between 70 and 110 km. Yuan et al. (2012) have shown that a significant decrease in Na abundance, compared to the climatological average, extended to mid-latitudes during a SSW event.

The major SSW in January 2009 has been reported as the strongest and most prolonged on record (Manney et al., 2009). In this paper, we report Na and Fe lidar observations made during this event, and use a combination of lidar measurements and global modelling to investigate the impact of a major SSW on the mesospheric Na, Fe, Mg and K layers. The neutral and ionic chemistries of these metals are different and so they have different responses to changes in atmospheric temperature

* Corresponding author.

E-mail address: J.M.C.Plane@leeds.ac.uk (J.M.C. Plane).<http://dx.doi.org/10.1016/j.jastp.2017.02.004>

Received 2 July 2016; Received in revised form 3 February 2017; Accepted 10 February 2017

1364-6826/ © 2017 The Author(s). Published by Elsevier Ltd.

This is an open access article under the CC BY-NC-ND license (<http://creativecommons.org/licenses/by-nc-nd/4.0/>).

and density (Plane et al., 2015). Measurements of temperature and the Na and Fe atom densities between 70 and 110 km were made at the Arctic Lidar Observatory for Middle Atmosphere Research (ALOMAR) in Northern Norway (69°N, 16°E) between 13 and 29 January 2009, covering the period of this major SSW. The resulting data set thus provides a valuable test of the model performance and the quality of the meteorological re-analysis data used to nudge the model. The paper is organized as follows: Sections 2 and 3 describe the measurements and model used in the study, respectively. Section 4 compares the model results with the lidar observations, and examines the impacts of the SSW on the four mesospheric metals. In Section 5 we present our summary and conclusions.

2. Lidar measurements

The sodium resonance lidar was installed at the ALOMAR observatory in Northern Norway (69°N, 16°E) in 2000 (She et al., 2002). The lidar measures temperature and Na density by probing the Doppler-broadened D2 line from roughly 80–105 km in altitude. Two stable infrared continuous-wave lasers (1064 nm and 1319 nm) are used to generate the sodium wavelength (589 nm) by sum-frequency generation. An acousto-optic modulator shifts the frequency alternately by +630 MHz, –630 MHz or 0 MHz relative to the D_{2a} emission line of sodium. The resulting beam is subsequently amplified in a pulsed Nd:YAG-pumped dye amplifier, before it is split into two steerable beams. Because no daylight filters were used in the receivers, the Na lidar was operated only in darkness during the time period of these observations.

The recently developed mobile iron lidar was installed at ALOMAR between June 2008 and July 2009. The lidar has measured Doppler temperatures and Fe density at mesopause altitudes with nearly seasonal coverage. Doppler resonance measurements are performed at the resonance line at 386 nm; in addition, aerosols above 20 km altitude are observed at 772 nm. In January 2009 the system was operating with a field of view (FOV) of 65 μ rad. The combination of the small FOV with daylight filters of 2.1 pm FWHM (386 nm) and 0.06 pm (772 nm) in the receiver allows measurements at day and night with negligible background. An earlier stage of the instrument is described in Höffner and Lautenbach (2009).

The photon count profiles taken with both lidars were analysed separately for temperature and metal density with a one hour integration time and 15 min time shift. The vertical resolution is 1 km in both cases. From these profiles three-hour mean values were calculated for each altitude with windows centred at midnight shifted by an integer times the length of the window. Values with statistical uncertainties in temperature larger than 10 K were ignored.

Analysis of the Na lidar data for temperature was complicated by the degradation of the seeder in the Nd:YAG pump laser shortly before these measurements started. As a result, two sidebands were generated in the spectrum of the amplified laser light. These additional laser lines introduced a priori an unknown shift in estimated mesospheric temperature. In principle, this temperature offset can be determined if the spectral width and amplitude of the sidebands are known. However, because the spectrum analyser which monitors the emitted laser beam was run only sporadically during the measurements reported here, we adopted a different approach to derive the Na lidar temperature. During the second half of January the Fe lidar was operated simultaneously with the Na lidar. Careful comparison of temperature profiles measured with both systems showed that the temperature offset observed with the Na lidar is (a) independent of altitude, and (b) constant in time. By evaluating the difference at 488 independent points totalling 42 h with simultaneous observations, the mean temperature offset was found to be 22.2 ± 7.3 K. A similar temperature comparison between Na lidar and the Rayleigh-Mie-Raman (RMR) lidar (Baumgarten, 2010) for 251 independent points totalling 47 h of observations showed that the mean temperature offset

was 21.7 ± 6.9 K. This independent comparison increases significantly the credibility of the Na temperature correction. The uncertainty is mainly caused by three factors. Firstly, because the Na and Fe lidars were pointed in different directions they did not observe a common volume of the atmosphere and hence the same wave effects. Secondly, the instruments took data that was not always simultaneous e.g., the beam of one instrument was blocked by clouds while the other instrument still received signal. The total Na lidar runtime in January 2009 was 99 h. For 37 h there were no simultaneous Fe lidar observations available. And finally, temperature measurements are not noise-free. Typical statistical uncertainties for the Na, Fe and RMR lidar measurements are 3–6 K over the altitude range (80–100 km) used for the comparison. Taking these factors into account, we believe that subtracting the estimated temperature offset (22.2 K) from the Na lidar temperatures reproduces the correct mesospheric temperatures measured by the Na lidar during the entire 17-day period discussed in this paper.

3. Model description

For this study we used the Whole Atmosphere Community Climate Model (WACCM) (Marsh et al., 2013b) with the inclusion of the chemistry of Na (Marsh et al., 2013a), Fe (Feng et al., 2013), Mg (Langowski et al., 2015) and K (Plane et al., 2014). The WACCM-Na chemistry is updated with new laboratory measurements of NaO and NaOH kinetics (Gómez Martín et al., 2016). WACCM-Fe is also updated with our recent work on the dissociative recombination of FeO^+ and photochemistry of FeOH (Bones et al., 2016; Viehl et al., 2016). WACCM is a high-top coupled chemistry-climate model with an upper boundary at 6.0×10^{-6} hPa (~ 140 km). The model horizontal resolution is $1.9^\circ \times 2.5^\circ$, with a vertical resolution in the MLT of ~ 3.5 km. In order to simulate the SSW event of January 2009, the specified dynamics version of WACCM was used where the model is nudged with NASA's Modern-Era Retrospective Analysis for Research and Applications (MERRA) (Lamarque et al., 2012) below 60 km. The reanalysis data was input every six hours. The Prandtl number (Pr), which governs the production of turbulence from breaking gravity waves, was set to 2 as the recommended standard value for upper atmospheric research (García et al., 2016). Therefore we use $\text{Pr}=2$ in the WACCM model runs described here, unless stated otherwise.

The meteoric input functions (MIFs) for the four metals are described in our recent papers (Feng et al., 2013; Marsh et al., 2013a; Plane et al., 2014; Langowski et al., 2015). It should be noted that vertical flux measurements of Na and Fe atoms indicate that these MIFs are most likely too low (Huang et al., 2015). This is probably because the horizontal resolution of WACCM is too coarse to explicitly resolve gravity waves with wavelengths less than ~ 100 km, so that WACCM may miss a significant component of the wave-driven chemical transport proposed by Gardner and Liu (2016). However, the magnitude of this unresolved chemical transport is unclear and needs to be the subject of future work. In the meantime, either the Na and Fe MIFs need to be scaled or the Prandtl number tuned to produce satisfactory WACCM simulations of the metallic layers at mid latitudes (see also section 4.2). The model output for the location of ALOMAR (69°N, 16°E) was sampled every 30 min.

4. Results and discussion

In this section the measured and simulated temperature, Na and Fe density in the MLT at ALOMAR during the 2009 SSW event are compared, before contrasting the modelled response of these metals with the Mg and K layers.

4.1. Meteorology

The major SSW in January 2009 has been described in Manney

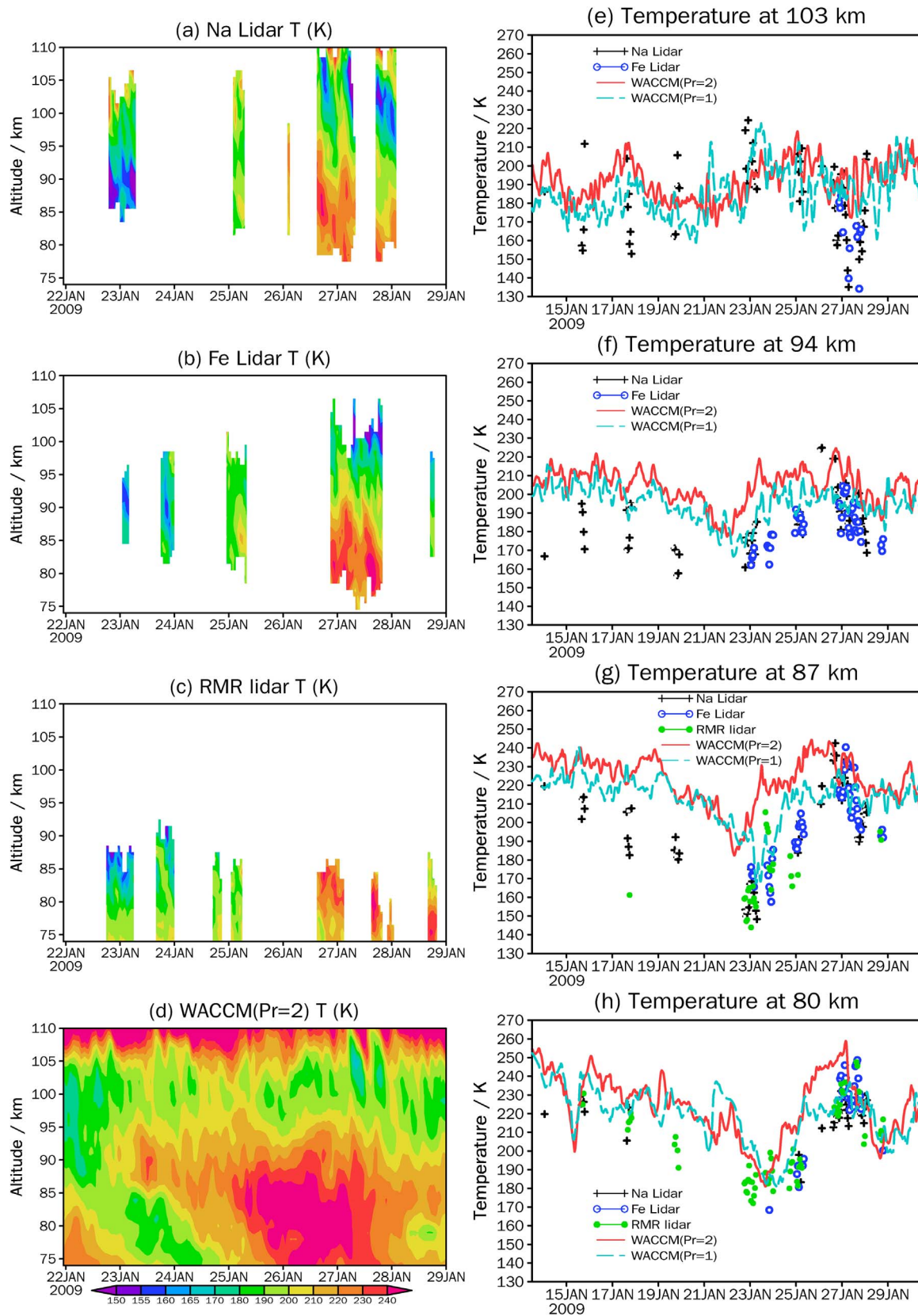


Fig. 1. Hourly averaged temperature profiles as a function of altitude (75–110 km) over ALOMAR station (69° N, 16° E), from 22 to 29 January 2009 and includes the time series of temperature at four selected altitudes from 13–30 January 2009: (a) Na lidar measurements; (b) Fe lidar measurements; (c) RMR lidar measurements; (d) WACCM (Pr=2) and WACCM (Pr=1) simulations, and temperatures at (e) 103 km; (f) 94 km; (g) 87 km and (h) 80 km.

et al. (2009). The zonal mean temperature at 60° N and 10 hPa increased rapidly from an average of 210 K up to 237 K on 23 January, with a reversal in the mean zonal wind on 24 January. Fig. 1 illustrates the hourly averaged temperature profiles measured at ALOMAR from 75 to 110 km by the Na and Fe lidars, and the RMR lidar below ~93 km, from 22 to 29 January 2009 and includes temperature time series at four selected altitudes (103 km, 94 km, 87 km and 80 km) from 13 to 30 January 2009 (note that the WACCM vertical resolution in the MLT is about 3.5 km). Exceptionally good weather conditions during this period allowed lidar observations almost every night. The Na lidar indicates the mesopause between 96 and 110 km between 15 and 19 January (not shown), with minimum temperatures ranging from 148–153 K (for example, at 103 km in Fig. 1e), which is much lower than the “normal” temperature (~190–210 K) in wintertime (January) estimated from lidar measurements by ignoring SSW and other unusual conditions (e.g., Neuber et al. (1988)). In contrast, during the SSW on 23 January the mesopause moved down to 89.5 km, with a minimum temperature as low as 137 K (Fig. 1a). After 27 January, the mesopause moved back up above 100 km (Fig. 1a). The Fe (Fig. 1b) and RMR (Fig. 1c) lidar temperature measurements are consistent with the low and very cold mesopause on 23 January, which are also clearly seen at 87 km (Fig. 1g).

Fig. 1(d–h) shows WACCM simulations at ALOMAR for the same period, with Pr set to either 2 or 1. The lower limit of Pr is 1 (Liu, 2009), which is chosen here for a model sensitivity experiment to assess the influence of vertical eddy diffusion on the temperature and metal layers in the MLT. Before 21 January, the modelled mesopause height is around 100 km in agreement with the observations, although the mesopause temperature between 170 and 190 K is ~20 K higher (not shown). The WACCM (Pr=2) model also overestimates the observed temperature at 94 km (Fig. 1f). The temperature falls to ~165 K above 87 km on 22–23 January; there is then a sharp temperature decrease around 75–85 km on 23–24 January (Fig. 1d, h) accompanied by the elevated stratopause temperature after the SSW. These changes were also seen in temperature profiles measured by satellites over this station (Singer et al., 2013). Although WACCM overestimates the observed mesopause temperatures at this location, the model captures well the timing of the mesospheric cooling. It should be noted that the modelled higher mesospheric temperatures do not result from nudging with the MERRA re-analysis data (which are known to be too warm in the mesosphere (Manney et al., 2008; Vignon and Mitchell, 2015)), because in the present study WACCM is free-running above 60 km. A low value of Pr=1 increases vertical eddy diffusion (e.g. Feng et al. (2013)). Changing the Pr value can also affect the energy balance between heating and cooling in the MLT (Huang and Smith, 1991). Setting Pr to the recommended value of 2 in WACCM gives colder temperature and shows better agreement with lidar measurement around 23 January 2009 (Fig. 1e–f).

In order to illustrate the thermal and wind structure changes in the MLT region during the SSW, Fig. 2 shows the time series of the zonally-averaged polar temperature, vertical, zonal and meridional wind from WACCM. The mesopause between 13 and 19 January occurs around 102 km with a temperature in the range 190–200 K, which is quite normal for polar winter, and is in line with other observations (e.g., (Neuber et al., 1988; Xu et al., 2007)). There is then a significant cooling of ~25 K between 78 and 102 km, which occurs mostly between 22 and 24 January. The modelled zonal mean temperature inside the high latitude at 87 km is about 10 K higher around 19 January and ~10–25 K lower from 23 to 28 January, compared with the temperature sampled at ALOMAR (not shown), which is due to the regional temperature variations (see Fig. 5 in Section 4.2). Although the modelled vertical wind (Fig. 2(b)) is quite noisy, there is generally descending air in the polar winter mesosphere before 17 January, followed by upward motion with a velocity as large as 4 cm s⁻¹ and associated adiabatic cooling (Fig. 2(a)). The zonal winds between 50 and 70°N are mainly eastwards (westerly) below 82 km before 20

January, which is normal for the northern hemisphere winter. However, the zonal wind reverses sign (i.e., changes to westward) on 21 January, with the strong westward winds reaching a peak speed of about -40 m s⁻¹ between 75 and 80 km on 22 January. After the SSW (i.e., from 24 January onwards), the winds throughout the MLT revert to eastward. The eastward winds in the lower mesosphere are much stronger than before the SSW, which is consistent with the results shown in long-term WACCM simulations by Holt et al. (2013). The meridional wind is much smaller than the zonal wind. There is a clear change in direction from the prevailing southerly wind to a northerly (i.e., equatorward) wind with speed of -12 m s⁻¹ between 81 and 96 km, between 21 and 24 January.

4.2. Impact on the Na and Fe layers

The mesospheric cooling caused by the SSW had a dramatic impact on the Na and Fe layers. Fig. 3 compares the time series of Na and Fe density measured by lidar between 70 and 110 km with the WACCM simulations sampled at the ALOMAR location. Here the WACCM simulations are plotted every thirty minutes while the observed Na and Fe are shown hourly (mainly for night time). In our previous studies with WACCM-Na (Marsh et al., 2013a) and WACCM-Fe (Feng et al., 2013), the MIFs were adjusted to give good fits to the mid-latitude metal layers. However, this resulted in the modelled layers in the polar winter being too concentrated compared to observations. Gardner et al. (2005) showed that the large enhancement of Na and Fe in the polar winter is most likely caused by convergence of air from lower latitudes at the top of the polar vortex. Hence, the WACCM over-prediction appears to arise because the modelled lifetimes of Na and Fe atoms in the MLT (~25 and 14 days, respectively) are too long (because vertical transport is underestimated – see Section 3), and/or convergence over the polar vortices is somewhat too strong. Therefore, in order to produce the best fit to the Na and Fe layer column abundances at ALOMAR during the entire observation period of the present study, we can either decrease the Na and Fe MIFs or increase vertical eddy diffusion in WACCM (for example, using Pr=1, the model is able to reproduce the observed lowest Na and Fe total column abundances during the SSW, which is clearly seen in Fig. 4). However, since a value of Pr=2 has been recently suggested as the standard for mesospheric work (Garcia et al., 2016), the MIFs were reduced by factors of 1.47 and 1.95, respectively, from the values in Marsh et al. (2013a) and Feng et al. (2013).

The observed Na layer occurs between 80 and 105 km in mid-late January with a peak Na density of ~5000 atom cm⁻³ around 90 km on 14 January, which slowly decreases to ~2000 atoms cm⁻³ on 19 January. However, there is then a sharp decrease down to less than 1000 atom cm⁻³ on 23 January. This large change in about ten days is roughly equivalent to the entire seasonal variation from winter to summer at this latitude (Marsh et al., 2013a). The measured Na peak density then recovers to a normal level above 5000 atoms cm⁻³ around 27 January. WACCM-Na captures quite well the changes in peak Na density and peak altitude during the SSW, in particular the sharp decrease of Na density around 22–23 January. Moreover, the model captures the unusually narrow Na layer around 22–23 January.

In the case of the Fe layer, the lidar measurements reveal a similar behaviour to Na, although there are few observations before 23 January. The observed Fe layer between 75 and 105 km is simulated satisfactorily by WACCM-Fe, particularly the large increase between 25 and 28 January around 85 km following the SSW. There are also pronounced diurnal variations on the bottom-sides of the Na and Fe layers below 76 km, in accord with lidar measurements at other locations reported by Kirchhoff et al. (1986), Yu et al. (2012) and Viehl et al. (2016), which are caused by photolysis and the reactions of H with the major reservoir species NaHCO₃ and FeOH (Yu et al., 2012; Plane et al., 2015; Viehl et al., 2016).

Fig. 4 shows the measured and modelled Na and Fe column

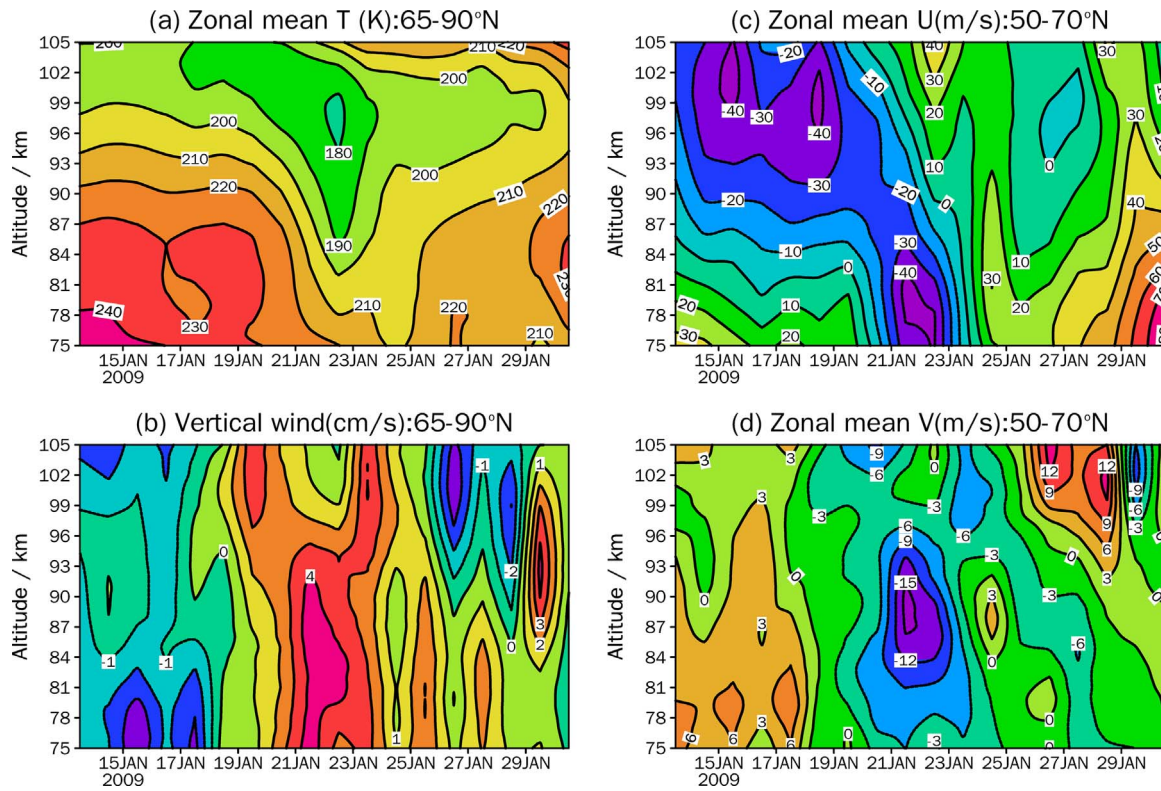


Fig. 2. WACCM (Pr=2) meteorological simulations between 75 and 105 km from 13 to 30 January 2009: (a) zonal mean temperature (65–90°N); zonal mean vertical wind (65–90°N); (c) zonal mean zonal wind (50–70°N); (d) zonal mean meridional wind (50–70°N).

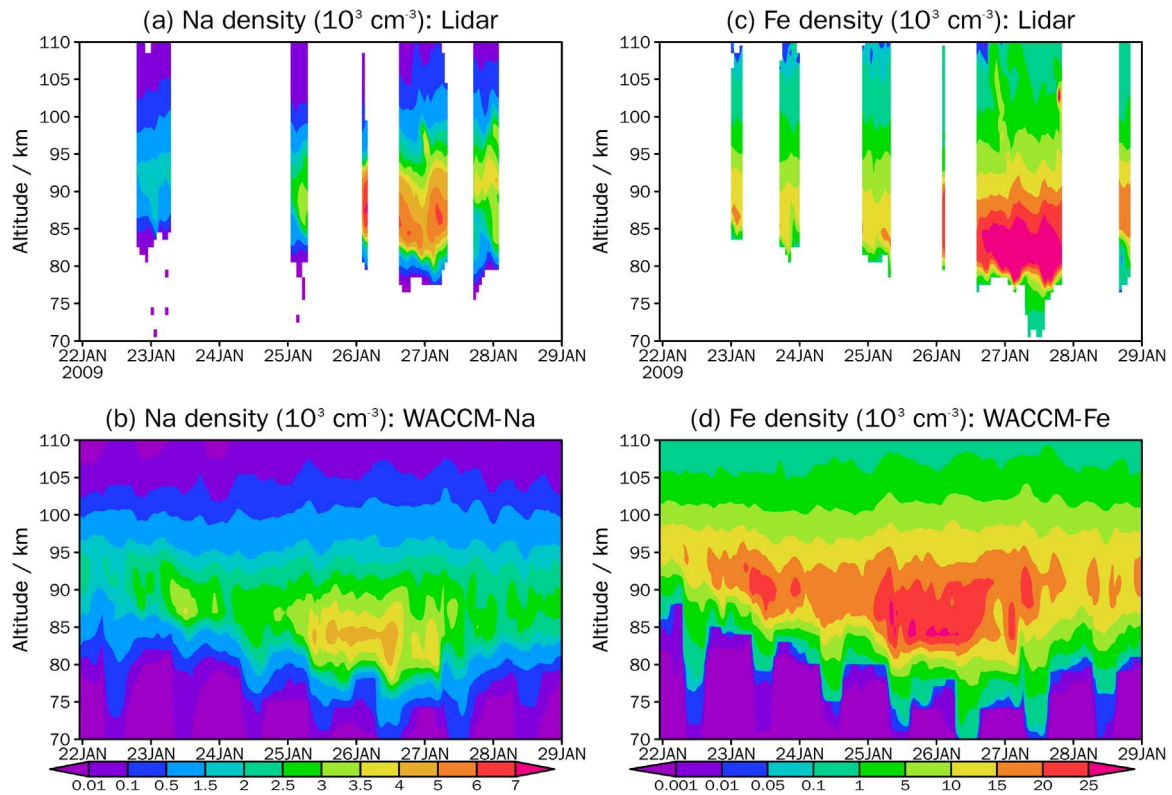


Fig. 3. Time series of the Na and Fe density between 70 and 110 km from lidar measurements and model (Pr=2) simulations sampled over ALOM station (69° N, 16° E). Note that the model results are scaled to match the entire measurement period (13–30 January 2009) by 1.47 and 1.95 for Na and Fe, respectively (see text).

abundances (integrated from 70 to 110 km). The measured Na column abundance decreases from mid-January to a minimum of $1.4 \times 10^9 \text{ cm}^{-2}$ on 22 January, before increasing rapidly by a factor of

~ 6.5 to $9 \times 10^9 \text{ cm}^{-2}$ on 27 January and returning to the mean value around $5 \times 10^9 \text{ cm}^{-2}$ on 28 January. The measured Fe column density decreased from $2.0 \times 10^{10} \text{ cm}^{-2}$ on 19 January to $1.2 \times 10^{10} \text{ cm}^{-2}$ on 25

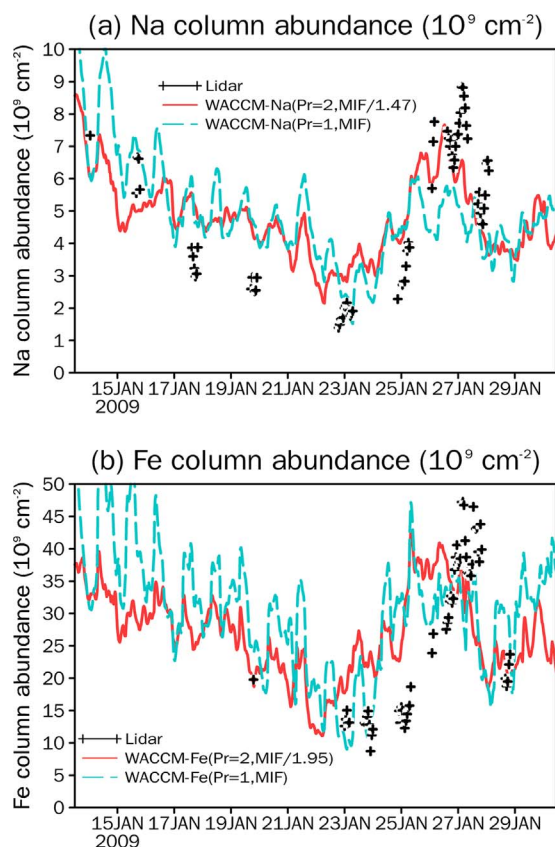


Fig. 4. Time series from 13–30 January 2009 of the observed and modelled column densities integrated from 70 to 110 km sampled over ALOMAR station (69° N , 16° E): (a) Na; (b) Fe. Note that the model (Pr=2) results are scaled to match the entire measurement period (13–30 January 2009) by 1.47 and 1.95 for Na and Fe, respectively (see text). The model simulations using Pr=1 with the MIF values of Na in Marsh et al. (2013a) and Fe in Feng et al. (2013) are also shown.

January before a dramatic increase to $4.5 \times 10^{10} \text{ cm}^{-2}$ on 28 January. The increases in the Na and Fe column abundance starting around 23 January are largely driven by the temperature increase at 87 km during the recovering phase of the SSW (cf. Fig. 4 with Fig. 1g). The strong positive correlation between temperature and number densities of Na and Fe around 87 km is a general feature, seen in both models and lidar measurements (e.g., (Feng et al., 2013; Dunker et al., 2015)). As shown in Fig. 1, the temperature increase in WACCM occurs 1–2 days earlier than observed by the lidars. Overall, WACCM captures the timing of these perturbations to Na and Fe during the SSW reasonably well, although the scale of the observed changes is about 20% larger than the model simulations for both metals. This is a consequence of the under-prediction of the extreme cooling during the SSW (Fig. 1). The largest vertical column density of Na from both measurement and model simulation around 26–27 January (also seen in the density profiles in Fig. 3) corresponds well with the high temperatures between 80 and 90 km (Fig. 1), which follows the elevated stratopause reforming after the major SSW (Holt et al., 2013). Again, using the MIF values of Na in Marsh et al. (2013a), and Fe in Feng et al. (2013), with Pr=1, the model is able to reproduce the observed lowest Na and Fe total column abundances during the SSW, but there are other discrepancies including more short-period variability than observed.

Marsh et al. (2013a) have shown that the SSW in January 2009 caused a short-term decrease in the total column abundances of Na over the polar cap ($> 70^\circ \text{ N}$). To further investigate the impact of the SSW on the hemispheric distribution of mesospheric metals, Fig. 5 shows the evolution of the modelled temperature, Na density and Fe density at 87 km every four days from mid to late January. The altitude of 87 km is close to the peak heights of these metal layers during the

event (Fig. 3), and the temperature also has a strong positive correlation with Na and Fe density at this level (Feng et al., 2013; Dunker et al., 2015). It should be noted that the hemispheric distributions of the column abundances of Na and Fe are very similar to their peak densities around 87 km. On 15 January the temperature at 87 km inside the polar region is above 220 K, which is reasonably typical for northern hemisphere winter. At mid-latitudes the temperature is generally lower, with a small cool area over North America. The warm polar air masses mainly move eastward on 19 January, with a large temperature decrease over North America. On 23 January there is an extensive band of cool air inside the polar region and most of mid-latitudes, along with two warm areas over Asia and the north Atlantic. In contrast, by 27 January following the SSW, the temperature has increased in patches inside the polar region.

The highest Na and Fe densities occur inside the polar vortex on 15 January. These high densities are caused by the meridional circulation which converges over the pole. This has two effects: Na and Fe atoms are transported from lower latitudes, and the local heating causes the release of Na and Fe from the reservoir species NaHCO_3 and FeOH (Gardner et al., 2005). Inspection of Fig. 5 shows that the modelled Na and Fe distributions correlate closely with temperature during the perturbations caused by the SSW. This correlation mostly arises because of the temperature-dependent neutral chemistry of both metals, which arises because the reactions which convert the metal reservoirs back to the metal atoms ($\text{NaHCO}_3 + \text{H} \rightarrow \text{Na} + \text{H}_2\text{CO}_3$ and $\text{FeOH} + \text{H} \rightarrow \text{Fe} + \text{H}_2\text{O}$) have activation energies close to 10 kJ mol^{-1} (Plane et al., 2015). These energies are large enough to cause a significant positive correlation between the metal atom concentration and temperature, because the reservoir species NaHCO_3 and FeOH are converted back to Na and Fe more rapidly at warmer temperatures. However, these energies are not so large ($> 15 \text{ kJ mol}^{-1}$) that the reactions are too slow over the mesospheric temperature range to have any significance, which is the case for the reaction of KHCO_3 with H (Plane et al., 2015). Na and Fe therefore also correlate closely with each other, although there are some differences. For example, a relatively significant Fe density over the Pacific Ocean on 15 January, and less of an increase in Fe over the Indian Ocean and part of Asia on 27 January, after the SSW.

4.3. Impact on the Mg and K layers

In general, the global distributions and vertical column densities of Na, K and Mg from WACCM agree well with the retrieved datasets from satellite measurements (Marsh et al., 2013a; Dawkins et al., 2015; Langowski et al., 2015). The simulated Na, Fe and K layers also agree reasonably well with lidar observations (Feng et al., 2013, 2015; Marsh et al., 2013a; Plane et al., 2014). Fig. 6 shows the percentage change in the modelled Na, Fe, Mg and K column abundances between 13 and 30 January as a function of latitude. It is clear that Mg behaves similarly to Na and Fe, while the perturbations to the K layer during and after the SSW are very different. Northward of 55° N there is a substantial decrease (up to $\sim 90\%$) in the column abundances of Na, Fe and Mg between 19 January and the peak of the SSW around 22 January, followed by a recovery after 25 January. Note that these metal layers are depleted first inside the polar region (also clearly seen in Fig. 5), and the depletion spreads to mid-latitudes ($40 - 55^\circ \text{ N}$) several days later. Between 15° and 40° N the model predicts the opposite behaviour: an increase of $\sim 30\%$ in column density from before the SSW to the peak around 22 January. Between 15° N and the equator, the increase in Na takes 2–5 days longer i.e. about 12 days after the peak enhancement at 80° N .

In contrast, Fig. 6(d) shows that the K column abundance increases over almost the entire northern hemisphere ($> 20^\circ \text{ N}$) during the SSW. This contrasting behaviour is due to the ion-molecule chemistry of K. The K^+ ion is much larger in size than Na^+ , and so the formation of cluster ions (e.g. $\text{K}^+ \cdot \text{N}_2$ and $\text{K}^+ \cdot \text{CO}_2$), which are the prelude to

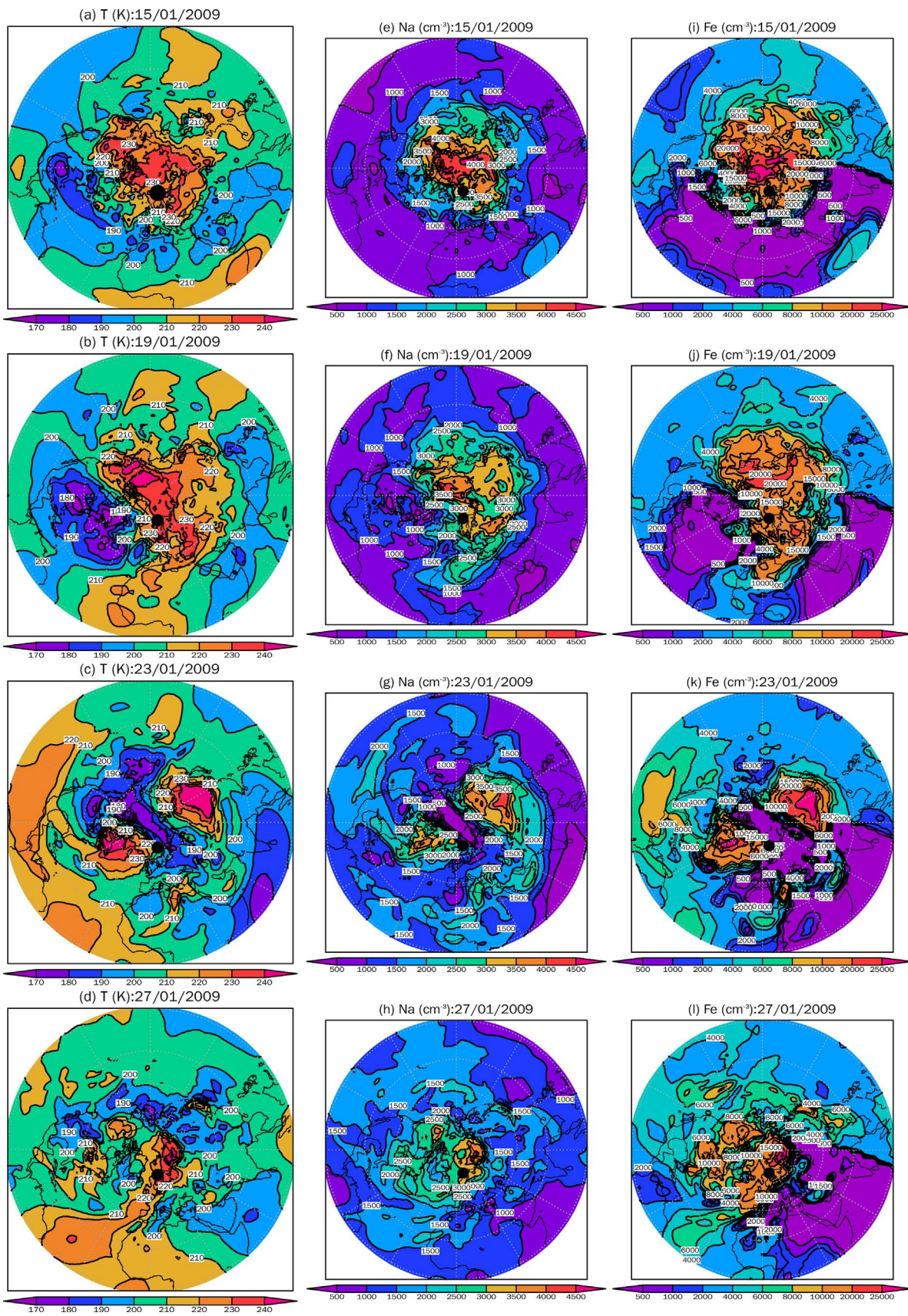


Fig. 5. Modelled (Pr=2) temperature (left panel), Na density (middle) and Fe density (right) at 87 km every four days from 15 January until 27 January in the Northern Hemisphere. The edge of each polar plot is the equator. Here the model output is saved at 0 Universal Time. The solid black circle in each map indicates the location of ALOMAR.

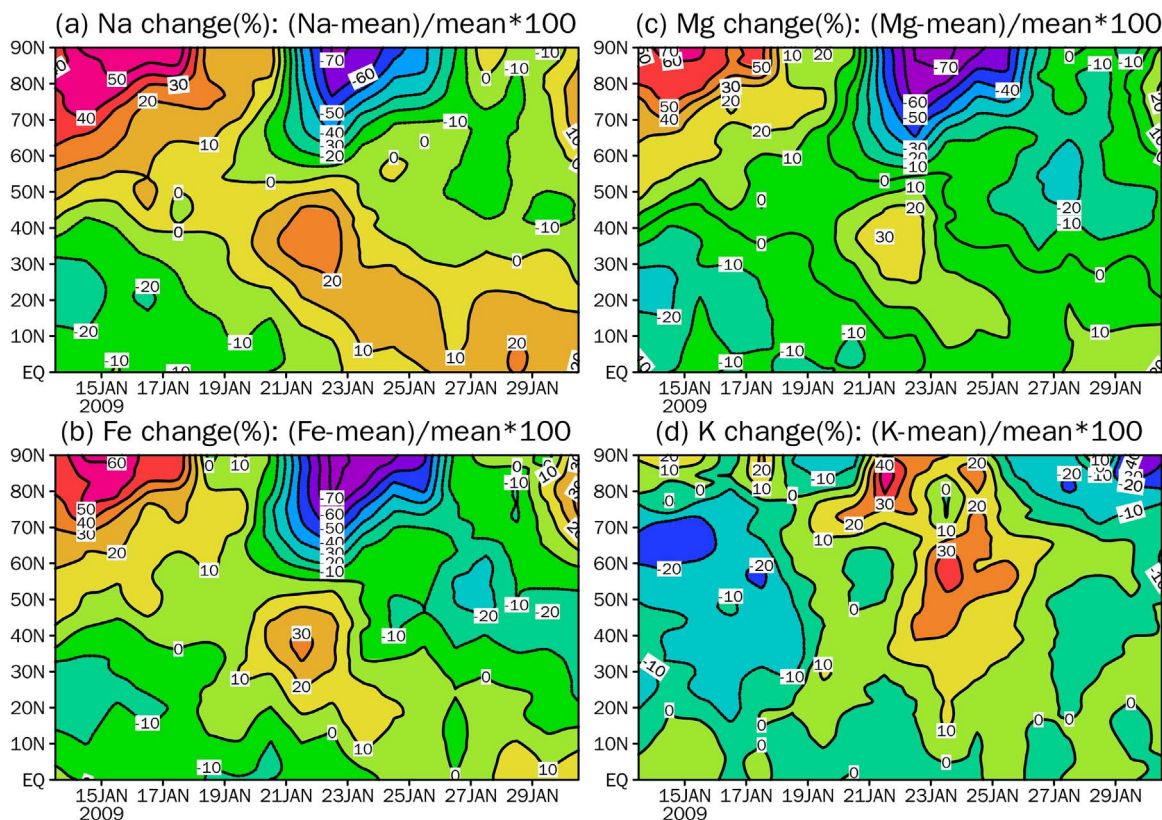


Fig. 6. Percent change of the modelled (Pr=2) metal column density with respect to the mean between 13 and 30 January, as a function of time and latitude (0–90° N): (a) Na; (b) Fe; (c) Mg; (d) K.

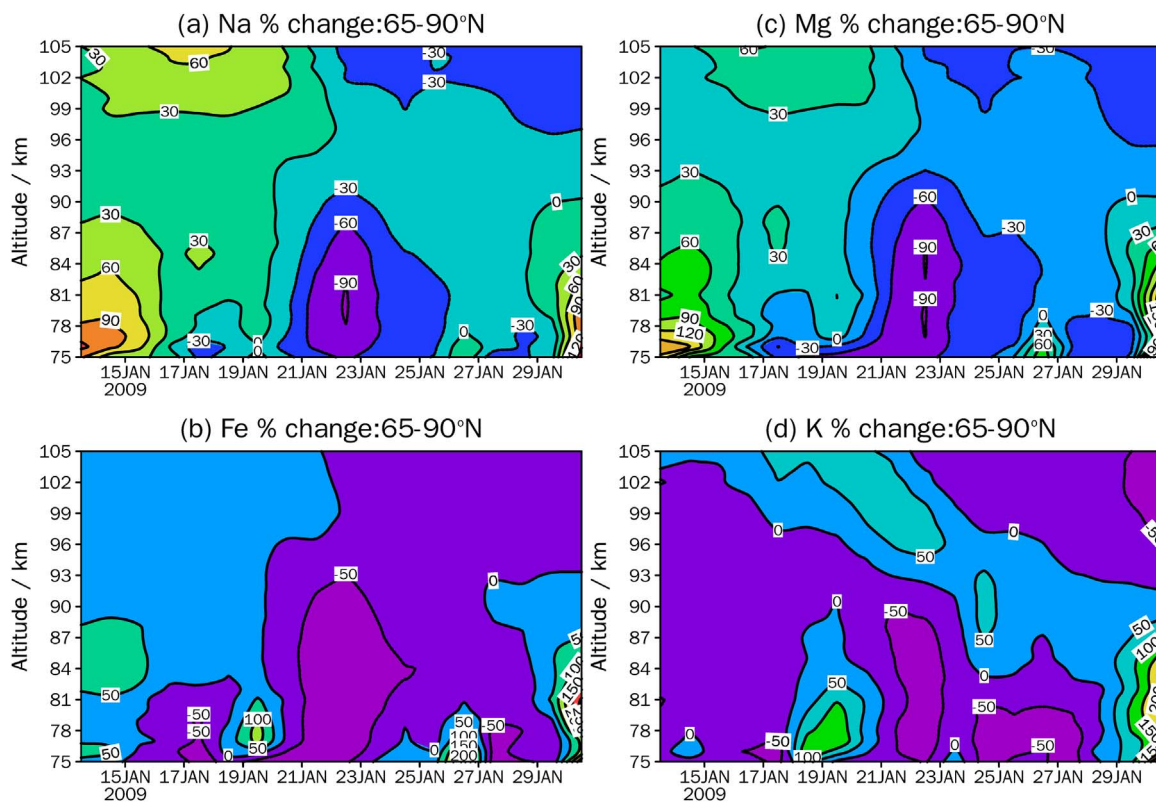


Fig. 7. Percent change of the modelled (Pr=2) metal density with respect to the mean between 13 and 30 January, as a function of time and height in the polar region (65 – 90° N): (a) Na; (b) Fe; (c) Mg; (d) K.

dissociative recombination with electrons to produce K, can only occur to a significant extent at very low temperatures (Plane et al., 2014). The substantial cooling of the MLT during the SSW thus converts this reservoir into K atoms. Fig. 7 shows the relative changes in the four metal layers as a function of altitude and time at polar latitudes. Na, Fe and Mg all decrease throughout the MLT during the SSW. In contrast, there is a substantial increase in K above 90 km on 22–23 January, as K^+ is converted to K, and this is nearly balanced by the decrease below 90 km caused by neutral chemistry (Fig. 7(d)). The net result is a small increase (< 20%) in the column abundance of K (Fig. 6(d)).

It should be noted that there are no measurements of metallic ions (or NO^+ and O_2^+) during the SSW with which to compare the WACCM simulations of these ionized species. However, Mg^+ is the one metal ion which can be observed globally by satellite during sunlit periods (hence not over ALOMAR during winter), and the WACCM modelled Mg^+ agrees very well with SCIAMACHY measurements up to 130 km (Langowski et al., 2015). We have also compared modelled Fe^+ , NO^+ , O_2^+ profiles with limited rocket-borne mass spectrometric measurements and show reasonable agreement (Feng et al., 2013): the model reproduces satisfactorily the Fe^+ peak layer and the underside of the layer, though overestimating the Fe^+ topside above 100 km (Bones et al., 2016). Moreover, WACCM captures well the measured $[Mg^+]/[Fe^+]$ ratio which is close to chondritic (Plane et al., 2016). Thus, despite the model lid at ~140 km and the absence of some electro-dynamical processes (Feng et al., 2013; Bones et al., 2016), WACCM appears to simulate the metallic ion layers below 120 km reasonably well.

5. Summary and conclusions

In the present study we have described lidar measurements of temperature, Na and Fe density in the MLT during a major SSW that occurred from mid to late January 2009. The observations record an exceptionally strong cooling above the ALOMAR observatory in northern Norway (69°N), with temperatures falling below 140 K on 22–23 January, coincident with maximum warming in the stratosphere. The observations demonstrate a strong correlation between temperature and the Na and Fe column densities. The chemistry-climate model WACCM, nudged below 60 km with reanalysis data but free running at higher altitudes, reproduces the timing of the SSW and the perturbations to the temperature, Na and Fe layers reasonably well. There is an under-prediction of the extreme cooling during the SSW, which leads to a small under-prediction of the observed ~80–90% decrease in the Na and Fe column abundances. The model is also used to show that this major SSW would have caused observable perturbations to the Na and Fe layers even at equatorial latitudes. The Mg layer is predicted to behave very like the Na and Fe layers, but the response of the K layer is quite different because of the conversion of K^+ ions into neutral K at the very low temperatures in the MLT during the SSW.

Acknowledgements

This work was supported by the European Research Council (project number 291332 – CODITA) and the UK Natural Environment Research Council (NERC grant NE/G019487/1). The National Center for Atmospheric Research is sponsored by the National Science Foundation. The Na lidar measurements were supported by the Research Council of Norway through grant 191755 and by US NSF grants AGS-0545262 and AGS-1136269. The lidar dataset is available upon request to B.K. and modelling output is available upon request to W.F. and J.M.C.P.

References

Baldwin, M.P., Dunkerton, T.J., 2001. Stratospheric harbingers of anomalous weather regimes. *Science* 294, 581–584.

- Baumgarten, G., 2010. Doppler Rayleigh/Mie/Raman lidar for wind and temperature measurements in the middle atmosphere up to 80 km. *Atmos. Meas. Tech.* 3, 1509–1518.
- Bones, D.L., Plane, J.M.C., Feng, W., 2016. Dissociative recombination of FeO^+ with electrons: implications for plasma layers in the ionosphere. *J. Phys. Chem. A* 120, 1369–1376.
- Butler, A.H., Seidel, D.J., Hardiman, S.C., Butchart, N., Birner, T., Match, A., 2015. Defining sudden stratospheric warmings. *Bull. Am. Meteor. Soc.* 96, 1913–1928.
- Chau, J.L., Fejer, B.G., Goncharenko, L.P., 2009. Quiet variability of equatorial E×B drifts during a sudden stratospheric warming event. *Geophys. Res. Lett.* 36, L05101.
- Christiansen, B., 2001. Downward propagation of zonal mean zonal wind anomalies from the stratosphere to the troposphere: model and reanalysis. *J. Geophys. Res.* 106, 27307–27322.
- Damiani, A., Funke, B., López Puertas, M., Gardini, A., von Clarmann, T., Santee, M.L., Froidevaux, L., Cordero, R.R., 2014. Changes in the composition of the northern polar upper stratosphere in February 2009 after a sudden stratospheric warming. *J. Geophys. Res.* 119, 11,429–411,444.
- Dawkins, E.C.M., Plane, J.M.C., Chipperfield, M.P., Feng, W., 2015. The near-global mesospheric potassium layer: observations and modeling. *J. Geophys. Res.* 120, 7975–7987.
- Dunker, T., Hoppe, U.-P., Feng, W., Plane, J.M.C., Marsh, D.R., 2015. Mesospheric temperatures and sodium properties measured with the ALOMAR Na lidar compared with WACCM. *J. Atmos. Sol.-Terr. Phys.* 127, 111–119.
- Feng, W., Höffner, J., Marsh, D.R., Chipperfield, M.P., Dawkins, E.C.M., Viehl, T.P., Plane, J.M.C., 2015. Diurnal variation of the potassium layer in the upper atmosphere. *Geophys. Res. Lett.* 42, 3619–3626.
- Feng, W., Marsh, D.R., Chipperfield, M.P., Janches, D., Höffner, J., Yi, F., Plane, J.M.C., 2013. A global atmospheric model of meteoric iron. *J. Geophys. Res.* 118, 9456–9474.
- Flury, T., Hocke, K., Haefele, A., Kämpfer, N., Lehmann, R., 2009. Ozone depletion, water vapor increase, and PSC generation at midlatitudes by the 2008 major stratospheric warming. *J. Geophys. Res.* 114, D18302.
- Garcia, R.R., López-Puertas, M., Funke, B., Kinnison, D.E., Marsh, D.R., Qian, L., 2016. On the secular trend of COx and CO₂ in the lower thermosphere. *J. Geophys. Res.* 121, 3634–3644.
- Gardner, C.S., Liu, A.Z., 2016. Chemical transport of neutral atmospheric constituents by waves and turbulence: theory and observations. *J. Geophys. Res.* 121, 494–520.
- Gardner, C.S., Plane, J.M.C., Pan, W., Vondrak, T., Murray, B.J., Chu, X., 2005. Seasonal variations of the Na and Fe layers at the South Pole and their implications for the chemistry and general circulation of the polar mesosphere. *J. Geophys. Res.* 110, D10302.
- Gómez Martín, J.C., Garraway, S.A., Plane, J.M.C., 2016. Reaction kinetics of meteoric sodium reservoirs in the upper atmosphere. *J. Phys. Chem. A* 120, 1330–1346.
- Goncharenko, L., Zhang, S.-R., 2008. Ionospheric signatures of sudden stratospheric warming: ion temperature at middle latitude. *Geophys. Res. Lett.* 35, L21103.
- Höffner, J., Lautenbach, J., 2009. Daylight measurements of mesopause temperature and vertical wind with the mobile scanning iron lidar. *Opt. Lett.* 34, 1351–1353.
- Holt, L.A., Randall, C.E., Peck, E.D., Marsh, D.R., Smith, A.K., Harvey, V.L., 2013. The influence of major sudden stratospheric warming and elevated stratosphere events on the effects of energetic particle precipitation in WACCM. *J. Geophys. Res.* 118, 11,636–611,646.
- Huang, T.Y.W., Smith, A.K., 1991. The mesospheric diabatic circulation and the parameterized thermal effect of gravity wave breaking on the circulation. *J. Atmos. Sci.* 48, 1093–1111.
- Huang, W., Chu, X., Gardner, C.S., Carrillo-Sánchez, J.D., Feng, W., Plane, J.M.C., Nesvorný, D., 2015. Measurements of the vertical fluxes of atomic Fe and Na at the mesopause: implications for the velocity of cosmic dust entering the atmosphere. *Geophys. Res. Lett.*, (2014GL062390).
- Kirchhoff, V.W.J.H., Batista, P.P., Clemesha, B.R., Simonich, D.M., 1986. The twilight sodium layer. *J. Geophys. Res.* 91, 13303–13307.
- Lamarque, J.F., Emmons, L.K., Hess, P.G., Kinnison, D.E., Tilmes, S., et al., 2012. CAM-chem: description and evaluation of interactive atmospheric chemistry in the Community Earth System Model. *Geosci. Model Dev.* 5, 369–411.
- Langowski, M., von Savigny, C., Burrows, J.P., Feng, W., Plane, J.M.C., et al., 2015. Global investigation of the Mg atom and ion layers using SCIAMACHY/Envisat observations between 70 km and 150 km altitude and WACCM-Mg model results. *Atmos. Chem. Phys.* 15, 273–295.
- Liu, A.Z., 2009. Estimate eddy diffusion coefficients from gravity wave vertical momentum and heat fluxes. *Geophys. Res. Lett.* 36, L08806.
- Liu, H., Doornbos, E., Yamamoto, M., Tulasi Ram, S., 2011. Strong thermospheric cooling during the 2009 major stratosphere warming. *Geophys. Res. Lett.* 38, L12102.
- Manney, G.L., Krüger, K., Pawson, S., Minschwaner, K., Schwartz, M.J., et al., 2008. The evolution of the stratopause during the 2006 major warming: satellite data and assimilated meteorological analyses. *J. Geophys. Res.* 113, D11115.
- Manney, G.L., Schwartz, M.J., Krüger, K., Santee, M.L., Pawson, S., Lee, J.N., Daffer, W.H., Fuller, R.A., Livesey, N.J., 2009. Aura Microwave Limb Sounder observations of dynamics and transport during the record-breaking 2009 Arctic stratospheric major warming. *Geophys. Res. Lett.* 36, L12815.
- Marsh, D.R., Janches, D., Feng, W., Plane, J.M.C., 2013a. A global model of meteoric sodium. *J. Geophys. Res.* 118, 11,442–411,452.
- Marsh, D.R., Mills, M.J., Kinnison, D.E., Lamarque, J.-F., Calvo, N., Polvani, L.M., 2013b. Climate Change from 1850 to 2005 Simulated in CESM1(WACCM). *J. Clim.* 26, 7372–7391.
- McInturff, R.M., 1978. Stratospheric warmings: synoptic, dynamic and general-circulation aspects. *NASA Ref. Publ.* 1017.

- Neuber, R., von der Gathen, P., von Zahn, U., 1988. Altitude and temperature of the mesopause at 69°N latitude in winter. *J. Geophys. Res.* 93, 11093–11101.
- O'Callaghan, A., Joshi, M., Stevens, D., Mitchell, D., 2014. The effects of different sudden stratospheric warming types on the ocean. *Geophys. Res. Lett.* 41, 7739–7745.
- Plane, J.M.C., Feng, W., Dawkins, E., Chipperfield, M.P., Höffner, J., Janches, D., Marsh, D.R., 2014. Resolving the strange behavior of extraterrestrial potassium in the upper atmosphere. *Geophys. Res. Lett.* 41, 4753–4760.
- Plane, J.M.C., Feng, W., Dawkins, E.C.M., 2015. The mesosphere and metals: chemistry and changes. *Chem. Rev.* 115, 4497–4541.
- Plane, J.M.C., Gómez-Martín, J.C., Feng, W., Janches, D., 2016. Silicon chemistry in the mesosphere and lower thermosphere. *J. Geophys. Res.* 121, 3718–3728.
- Rose, K., Brasseur, G., 1989. A three-dimensional model of chemically active trace species in the middle atmosphere during disturbed winter conditions. *J. Geophys. Res.* 94, 16387–16403.
- She, C.Y., Vance, J.D., Williams, B.P., Krueger, D.A., Moosmüller, H., Gibson-Wilde, D., Fritts, D., 2002. Lidar studies of atmospheric dynamics near polar mesopause. *EOS Trans. Am. Geophys. Union* 83, 289–293.
- Singer, W., Hoffmann, P., Kishore Kumar, G., Mitchell, N.J., Matthias, V., 2013. Atmospheric coupling by gravity waves: climatology of gravity wave activity, mesospheric turbulence and their relations to solar activity. In: Lübken, F.-J. (Ed.), *Climate and Weather of the Sun-Earth System (CAWSES): Highlights From a Priority Program*. 409–427. Springer, Netherlands.
- Viehl, T.P., Plane, J.M.C., Feng, W., Höffner, J., 2016. The photolysis of FeOH and its effect on the bottomside of the mesospheric Fe layer. *Geophys. Res. Lett.* 43, 1373–1381.
- Vignon, E., Mitchell, D.M., 2015. The stratopause evolution during different types of sudden stratospheric warming event. *Clim. Dyn.* 44, 3323–3337.
- Vincent, R.A., 2015. The dynamics of the mesosphere and lower thermosphere: a brief review. *Prog. Earth Planet. Sci.* 2, 1–13.
- Xu, J., Liu, H.L., Yuan, W., Smith, A.K., Roble, R.G., Mertens, C.J., Russell, J.M., Mlynczak, M.G., 2007. Mesopause structure from Thermosphere, Ionosphere, Mesosphere, Energetics, and Dynamics (TIMED)/Sounding of the Atmosphere Using Broadband Emission Radiometry (SABER) observations. *J. Geophys. Res.* 112, D09102.
- Yamashita, C., Liu, H.-L., Chu, X., 2010. Gravity wave variations during the 2009 stratospheric sudden warming as revealed by ECMWF-T799 and observations. *Geophys. Res. Lett.* 37, L22806.
- Yamazaki, Y., Kosch, M.J., Emmert, J.T., 2015. Evidence for stratospheric sudden warming effects on the upper thermosphere derived from satellite orbital decay data during 1967–2013. *Geophys. Res. Lett.* 42, 6180–6188.
- Yu, Z., Chu, X., Huang, W., Fong, W., Roberts, B.R., 2012. Diurnal variations of the Fe layer in the mesosphere and lower thermosphere: four season variability and solar effects on the layer bottomside at McMurdo (77.8°S, 166.7°E), Antarctica. *J. Geophys. Res.* 117, D22302.
- Yuan, T., Thurairajah, B., She, C.Y., Chandran, A., Collins, R.L., Krueger, D.A., 2012. Wind and temperature response of midlatitude mesopause region to the 2009 sudden stratospheric warming. *J. Geophys. Res.* 117, D09114.